Desalination and Water Treatment
www.deswater.com

doi:10.5004/dwt.2019.23475

141 (2019) 229–237
February

Synthesis of magnetic Fe_3O_4/hydroxyapatite nanocomposites and adsorption to Cu^{2+} ions

Zhaoxia Hou*, Chunhan Zhang, Haibo Long, Meihan Wang, Xiaodan Hu

[a]*Liaoning Province Key Laboratory of New Functional Materials and Chemical Technology, School of Mechanical Engineering, Shenyang University, Shenyang 110044, China, email: luckyxia2007@126.com (Z. Hou), 1159642856@qq.com (C. Zhang), 46905476@qq.com (H. Long), 2282642664@qq.com (M. Wang), 2684282072@qq.com (X. Hu)*

Received 21 June 2018; Accepted 18 November 2018

ABSTRACT

In the paper, magnetic Fe_3O_4/Hydroxyapatite (Fe_3O_4/HA) nanocomposites were prepared by a mechanical method and an in-situ method. XRD and SEM were used to characterize the microstructure and morphology. The adsorption performance of bare HA as well as the magnetic Fe_3O_4/HA nanocomposites to Cu^{2+} ions were investigated and compared. The results showed that the particle size of magnetic Fe_3O_4/HA nanocomposites synthesized in-situ had a uniform distribution. The crystallinity and the particle size were found to increase with the molar ratio of Fe_3O_4: HA and the hydrothermal reaction temperature. The magnetic Fe_3O_4/HA nanocomposites prepared by the two methods both have the ability to absorb Cu^{2+} ions. The removal efficiency of magnetic Fe_3O_4/HA nanocomposites in-situ to Cu^{2+} ions is 95%, higher than those by the mechanical method (91%). The adsorption capacity of Fe_3O_4/HA in-situ is higher than that mechanically and bare HA. The magnetic Fe_3O_4/HA nanocomposites can be completely separated by external magnetic field, so it has the potential of practical application in the heavy metal wastewater treatment.

Keywords: Magnetic nanocomposites; Hydroxyapatite; In-situ synthesis; Cu^{2+} ions; Adsorption

1. Introduction

With increasing amount of heavy metal pollution in global water, how to mitigate the heavy metal pollution in water resources has become a top priority for research scientists. The heavy metal pollution treatment technologies can be classified into three categories: chemical precipitation, physical chemistry and biological method [1]. The adsorption method removes heavy metal ions through the strong affinity between the heavy metal pollutants and the adsorbent. Adsorption method is a convenient and effective method with the advantages of simple and convenient operation, good removal efficiency, easy recovery of heavy metal ions, no or little secondary pollution, a wide range of material sources and low cost, etc. [2]. Therefore, it attracts broad academic interest to develop adsorbents that are simpler and cheaper, and can be used repeatedly.

Natural mineral materials such as zeolite, smectite, rectorite, diatomite and apatite have been gradually developed for the adsorbent materials [3–7]. They have advantages such as extensive resources, low cost, and no secondary pollution in heavy metal wastewater treatment and soil remediation compared with other types of adsorbents. Hydroxyapatite (HA) has achieved good results in adsorption of heavy metal ions due to its special crystal structure, good ion exchange and thermal stability, and become a new environmental protection functional material [8,9]. HA has a wide range of acceptability for heavy metal ions and is easy to be synthesized [10,11], therefore, it has great potential value in wastewater treatment. However, it is difficult to be separated completely from the waste water due to its powdery appearance and poor mechanical properties, which limits its practical application.

Magnetic separation technology has emerged as a physical separation method in industrial wastewater treatment. Fe_3O_4 is a traditional magnetic material with the advantages

*Corresponding author.

of large specific surface area, high reactivity, low preparation cost and high efficiency. Its unique magnetic properties make it widely used in various fields. Since the beginning of the 20th century, the magnetic properties and electrical properties of Fe_3O_4 particles have attracted the attention of researchers in various fields, Fe_3O_4 has been widely used in magnetic fluids, magnetic records, magnetic refrigeration, catalysts, medicine and construction [12–16]. At present, its excellent magnetic properties, high specific surface activity and biocompatibility have enabled it to be used as an adsorbent in the treatment of heavy metal ions. Z. Chen et al. used the electronegativity of the surface of Fe_3O_4 nanoparticles to adsorb heavy metal ions in the wastewater [17]. Magnetic adsorbents have the characteristics of easy recycling and excellent adsorption performance, and are considered as a green and environmentally friendly adsorbent [18,19]. High-performance adsorption and magnetic recovery properties can be achieved by combining magnetic Fe_3O_4 with other materials. It has the great potential in the treatment of wastewater, and the heavy metals can be recovered and no secondary pollution occurs.

Our research group has conducted some work on the adsorption performance of HA and modified HA to heavy metal ions in recent years [20–25]. The effects of pH, temperature and adsorption time have been investigated in previous work. We found that: at low pH, a large amount of H^+ and Cu^{2+} ions in the solution can be adsorbed on the active sites. HA has a small amount of dissolution, the Ca^{2+} dissolved will not make effect to adsorb Cu^{2+} ions, so the removal rate is not very high; when 3 < pH < 7, as the pH value increases, the negative charge on the surface of HA increases, which is favorable for the adsorption of cations on the surface of HA, and the removal rate to Cu^{2+} ions shows an upward trend; when 7 < pH < 8, the removal rate begins to decrease; when pH = 9, the removal rate slightly increased because of the precipitation of $Cu(OH)_2$. In general, when the pH ≥ 3, the removal rate is on the high level, the adsorption of Cu^{2+} ions by HA has a wide pH range. Here, pH = 7 is carried out based on two considerations: (1) the best adsorption performance under pH = 7 condition according to previous research, (2) its ease to operate for no need to add acid or alkali to adjust the pH value. With the increase of temperature, the removal rate of Cu^{2+} ions increases, especially between 20~40°C and slower after 40°C. However, considering the actual situation, it is generally preferred to carry out adsorption at room temperature, so adsorption experiments were carried out at room temperature here. This work focuses on the magnetic Fe_3O_4/HA nanocomposites synthesized mechanically and in-situ for the removal of Cu^{2+} from aqueous solution. The composite adsorbent can be magnetized under an external magnetic field, thereby facilitating the separation, recycling and reuse of the adsorbent.

2. Experimental

2.1. Materials

All commercial reagents such as $CaNO_3{\cdot}4H_2O$, $(NH_4)_2HPO_4$, $C_{12}H_{22}SO_4Na$ (SDS), $FeCl_3{\cdot}6H_2O$ and $FeCl_2{\cdot}4H_2O$ etc. are all analytical grade and used directly without any further purification.

2.2. Preparation of Fe_3O_4/HA nanocomposites

In the in-situ method, the anionic template SDS 5 g was dissolved in 60 mL ethanol/water (1:1, v/v) solution and preheated to 60°C to fully dissolve. $FeCl_3{\cdot}6H_2O$ and $FeCl_2{\cdot}4H_2O$ in the molar ratio of 2:1 were dissolved in 40 mL ethanol/water (1:1, v/v) solution and heated to 60°C, and then mixed with the SDS solution above (marked as Solution A). 2 M NaOH solution was injected into the solution A with a syringe to control the pH > 11. 2 g NaOH and 0.03 mol $(NH_4)_2HPO_4$ were dissolved in 60 mL ethanol/water (1:1, v/v) solution and preheated to 60°C. Under nitrogen protection, 60 mL $Ca(NO_3)_2$ solution with pH > 11 was added drop wise into $(NH_4)_2HPO_4$ solution with stirring at 60°C for 30 min (marked as Solution B). The molar ratio of Ca:P is 5:3. The molar ratio of $(Fe^{2+}+Fe^{3+}):Ca^{2+}$ is 3:10, 3:20 and 3:30, respectively. The solution A and B were poured into PTFE reactors and heated at 60°C for 12 h. After cooling to room temperature, it was washed with ethanol and water until neutral. Powder was vacuum dried at 55°C for 24 h. Fe_3O_4/HA composites were obtained after the template was removed by vacuum sintering at 600°C. The above experiments were repeated with the hydrothermal temperature at 80°C and 120°C for 12 h, respectively. In addition, bare Fe_3O_4 and HA were separately synthesized using the same process. Fe_3O_4/HA nanocomposites in-situ marked as molar ratio (Fe_3O_4:HA)@hydrothermal temperature. For example 1:1@60°C represents the molar ratio of Fe_3O_4:HA is 1:1 and hydrothermal temperature is 60°C.

In the mechanical method, bare Fe_3O_4 and HA were mechanically mixed with the molar ratio of Fe_3O_4:HA = 1:1, 1:2, 1:3, respectively. Deionized water was used as the dispersant, and the resulting suspension was stirred at 60°C for 90 min at a nitrogen atmosphere, then magnetic separation was performed. The dark brown magnetic Fe_3O_4/HA composite powders were obtained after drying under vacuum at 55°C for 24 h. Fe_3O_4/HA nanocomposites prepared mechanically marked as M-1:1, M-1:2 and M-1:3 according to the molar ratio of Fe_3O_4 to HA, respectively.

2.3. Adsorption experiments

Adsorption experiments were carried out in batch at room temperature. The concentration of adsorbent and Cu^{2+} are 2 g/L and 20 mg/L, respectively, and pH value is 7. After different adsorption duration, magnetic separation was performed using a magnet, and then the supernatant was filtered and diluted with 1% HNO_3 solution, which was used to measure the concentration of Cu^{2+} residue. All experimental data were in triplicate and finally averaged.

2.4. Characterization

X-ray diffraction (XRD, PANalytical, Holland) was analyzed by Cu Kα radiation (λ = 0.15418 nm) at 40 kV and 40 mA from 20° to 70°. The scanning speed is 10°/min at the step length of 0.03°. The microstructure and morphology were observed by a Field Emission Scanning Electron Microscope (FE-SEM, HitachiS4800, Japan). Before the SEM measurement, samples were sputtered with gold by an ion sputter device (E-1045, Hitachi, Japan). The concentration

of Cu^{2+} was measured by atomic adsorption spectroscopy (AAS, Varian AA220, USA).

The removal efficiency was calculated using the following equation:

$$Y = \frac{C_0 - C_e}{C_0} \times 100\% \quad (1)$$

where Y is the removal efficiency(%), C_0 and C_e are the concentration (mg/L)of Cu^{2+} ions in solution before and after adsorption.

The adsorption capacity was calculated using the following equation:

$$Q = \frac{(C_0 - C_e) \times V}{m} \quad (2)$$

where Q is the adsorption capacity (mg/g), V is the volume of the solution (L), m is the amount of HA in the adsorbent (g).

Pseudo-first-order kinetic model used to describe the solid-liquid adsorption process is shown in Eq. (3),

$$\ln(Q_e - Q_t) = \ln Q_e - k_1 t \quad (3)$$

The pseudo-second kinetic model is based on Eq. (4),

$$t / Q_t = (1 / k_2 Q_e^2) + t / Q_e \quad (4)$$

The intraparticle diffusion model was proposed by Weber and Morris, and its expression is:

$$Q_t = k_{id} t^{1/2} + I \quad (5)$$

where Q_t is the amount of adsorption at t time (mg /g), Q_e is the balanced adsorption amount (mg/g), k_1 is the first-order adsorption rate constant (min^{-1}), k_2 is the second-order adsorption rate constant (g/mg·min^{-1}), t is the adsorption time (min), k_{id} is the intraparticle diffusion rate constant, and I is the thickness of the boundary layer.

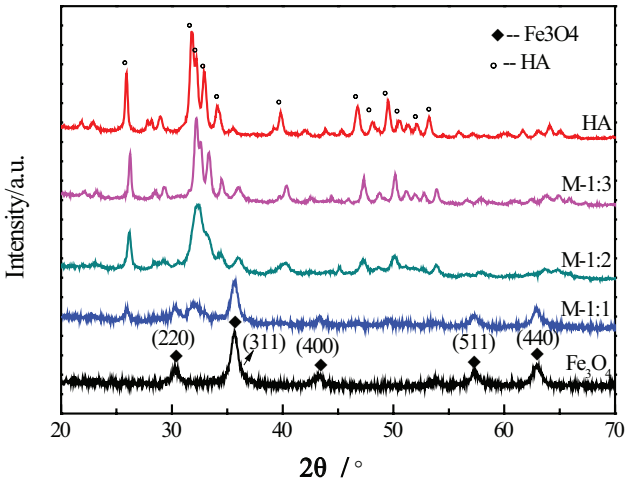

Fig. 1. XRD patterns of HA, Fe_3O_4 and Fe_3O_4/HA prepared by mechanical mixing method.

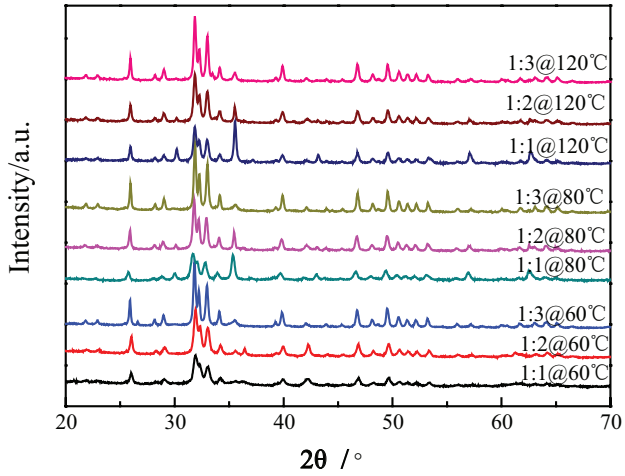

Fig. 2. XRD patterns of Fe_3O_4/HA synthesized in-situ.

3. Results and discussion

3.1. Microstructure and morphology

XRD patterns of HA, Fe_3O_4 and Fe_3O_4/HA nanocomposites (M-1:1, M-1:2, M-1:3) prepared mechanically are shown in Fig. 1. The diffraction peaks of HA at 25.8°, 31.8°, 46.9° and 49.7° are corresponding to the (002), (211), (222) and (213) according to JCPDS 76-0694. It is noticed that all diffraction peaks of Fe_3O_4 at 30.2°, 35.6°, 43.2°, 53.7°, 57.2° and 62.7° can be indexed to face-centered cubic magnetite (JCPDS No. 85-1436), and are corresponding to (220), (311), (400), (422), (511) and (440) planes, respectively. XRD patterns of Fe_3O_4/HA nanocomposites combine $Fe_3O_4$with HA, which indicates that magnetic Fe_3O_4/HA nanocomposites were successfully prepared mechanically. For M-1:1, due to the high content of Fe_3O_4, the diffraction peak of Fe_3O_4 is strong and sharp, and become the main crystal phase, while HA is the secondary crystal phase. With the increase of HA content, HA diffraction peak become stronger and sharper than Fe_3O_4, and the peak shape of M-1:2 and M-1:3 is more similar with the pattern of bare HA.

XRD patterns of Fe_3O_4/HA nanocomposites synthesized in-situ are shown in Fig. 2. There are difference among the XRD patterns due to the different hydrothermal temperature and molar ratio of Fe_3O_4 to HA. It can be seen that all the diffraction peaks correspond to the characteristic peaks of Fe_3O_4 or HA, and no other peaks can be observed. The results show that magnetic Fe_3O_4/HA nanocomposites were successfully synthesized by the in-situ synthesis method. The diffraction peaks of Fe_3O_4/HA nanocomposites appear narrower, stronger and sharper with the hydrothermal temperature increase from 60°C to 120°C. It can be explained that the grain growth rate is accelerated with the increase of temperature, which is consistent with the results of SEM later.

It can be seen from Fig. 2 that the main crystal phase is HA and secondary crystal phase is $Fe_3O_4$for all samples except 1:1@80°C and 1:1@120°C, which indicates that the

hydrothermal temperature and molar ratio can influent the phase composition. The diffraction peaks at 31.5° and 32.8° split clearly and become sharper with the increase of HA content, which indicates that the powder crystallizes to a higher degree. It may be explained that Fe_3O_4 nanoparticles cause heterogeneous nucleation. HA coats on the surface of Fe_3O_4 nanoparticles acting as the nucleus, more and more HA precipitates on the surface of Fe_3O_4 with the increase of HA content, so leading to the increase of the composite particle size.

SEM images of bare HA, bare Fe_3O_4 and Fe_3O_4/HA nanocomposites synthesized mechanically are shown in Fig. 3. HA (Fig. 3a) appears as short nanorods and the particle size distributes uniformly. Fe_3O_4 (Fig. 3b) appears nanospheres with the particle size of 20–40 nm, and a little aggregation is visible. The short HA nanorods and the Fe_3O_4 nanospheres can be seen from Figs. 3c, d and e, which indicates that there is no chemical action between the Fe_3O_4 and HA in the mechanical mixing process. With the increase of the HA' content, particle agglomeration phenomenon decreases and the dispersibility becomes better.

SEM images of Fe_3O_4/HA synthesized in-situ are shown in Fig. 4. The Fe_3O_4/HA nanocomposites appear as short nanorods. Both the particle size and the aggregation degree increase with the increase of hydrothermal temperature and HA' content. Compared the particle size

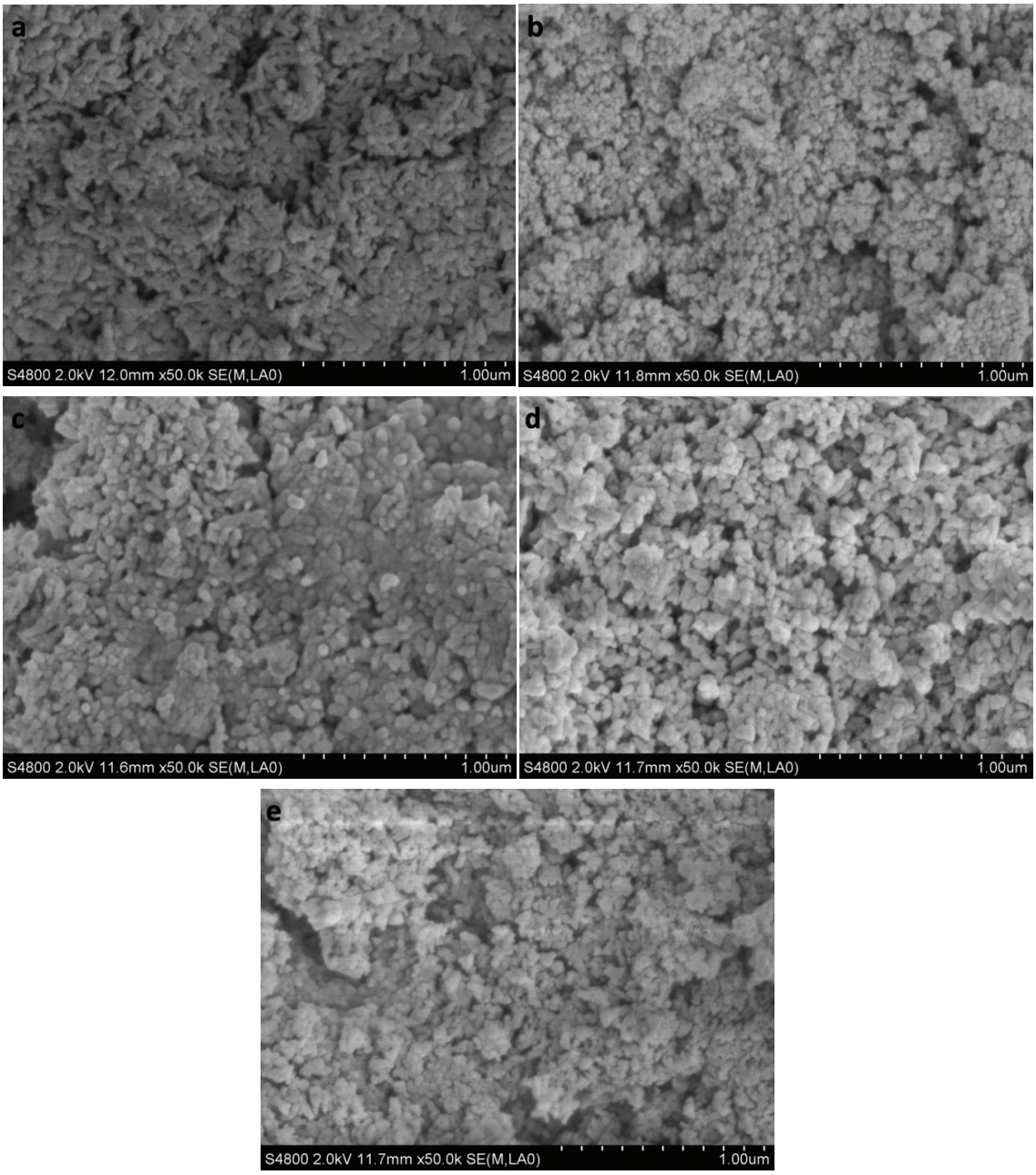

Fig. 3. Micromorphology of bare HA (a), bare Fe_3O_4(b) and Fe_3O_4/HA (c,d,e) synthesized mechanically.

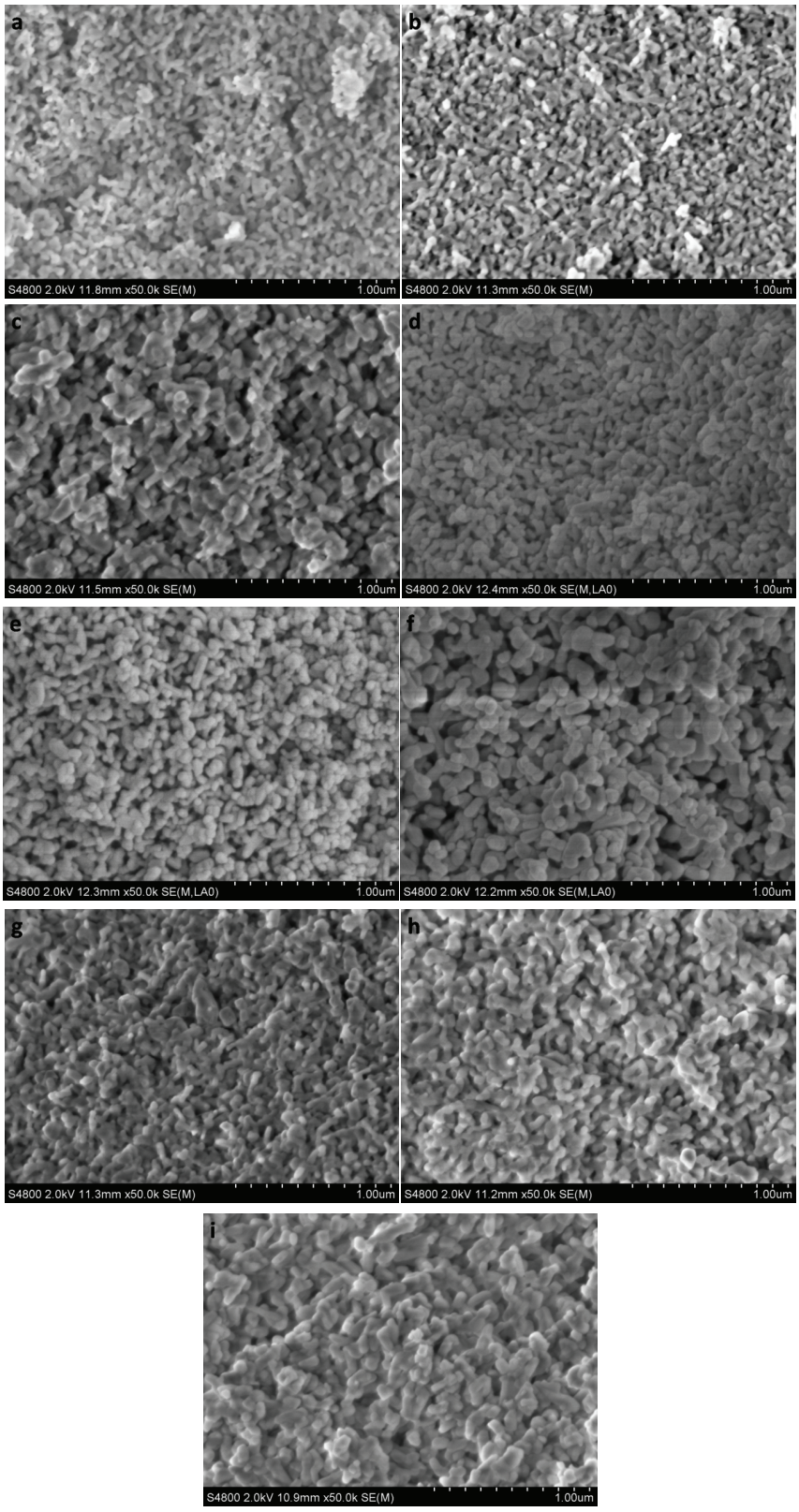

Fig. 4. Micromorphology of Fe_3O_4/HA synthesized in-situ. (a) 1:1@60°C; (b) 1:2@60°C; (c) 1:3@60°C; (d) 1:1@80°C; (e) 1:2@80°C; (f) 1:3@80°C; (g) 1:1@120°C; (h) 1:2@120°C; (i) 1:3@120°C.

of Fe_3O_4/HA naocomposites under same molar ratio, samples at 60°C has the smallest size with larger specific surface area and better dispersibility, which can provide more adsorption sites and facilitate the removal of heavy metal ions, it will be testified by follow-up adsorption performance discussion. Comparing the morphology of the samples synthesized at same temperature, the particle size and aggregation degree increases with the increase of HA' content.

3.2. Magnetic property and adsorption performance

In order to test the magnetic property of the Fe_3O_4/HA nanocomposites, a simple magnet experiment was performed. 0.2 g Fe_3O_4/HA nanocomposites M-1:1 (Fig. 5a) and 1:1@60°C (Fig. 5c) are dispersed ultrasonicly in deionized water for 30 min, respectively. Fe_3O_4/HA nanocomposites were quickly attracted to the magnet side after applying an external magnetic field by a rubidium magnet for 2 min, as shown in Figs. 5b,d. The obvious magnetic response indicates that the Fe_3O_4/HA nanocomposites prepared mechanically and in-situ are magnetic . Comparing Fig. 5b with 5d, it can be found that the supernatant of Fe_3O_4/HA nanocomposites prepared in-situ was clearer, which indicates that its magnetic separation is more thorough. It can be explained that the HA coated completely on the Fe_3O_4 nucleus by in-situ method, while mechanical mixing method may not combine the HA with Fe_3O_4uniformly. HA is not magnetic, the magnetic property of composite particles are completely caused by the super paramagnetism of Fe_3O_4, which proves that Fe_3O_4 is successfully compounded with HA by in-situ method, and can be quickly removed under the magnetic field conditions.

The removal efficiency of bare HA and Fe_3O_4/HA nanocomposites synthesized mechanically and in-situ to Cu^{2+} were investigated at different adsorption time, and shown in Fig. 6. It can be seen from Fig. 6 that the adsorption capacity of Fe_3O_4/HA M-1:3 is significantly better than that of M-1:1 and 1:2, and the saturation removal efficiency reaches 91%. Under the same molar ratio 1:2 condition, the removal efficiency of 1:2@60°C to Cu^{2+} ions is higher than that of 1:2@80°C, and 1:2@120°C is the lowest. As the hydrothermal temperature increases, the degree of crystallization and agglomeration increases, the particle size becomes larger, which results in the decrease of the specific surface area, so the adsorption active sites decrease and lead to the decrease of the removal efficiency.

Comparing the adsorption curves of Fe_3O_4/HA synthesized in-situ at 60°C, the saturation removal efficiency of 1:2@60°C is the highest, about 95%, and 1:3@60°C is the lowest, about 62%. This is due to that the crystallinity is greatly increased with the increase of HA' content. The sintered neck forms between particles and particles become bigger and coarser, thus leads to a decrease in the specific surface area, and therefore the adsorption effect is significantly reduced. However, the removal efficiency of 1:1@60°C is not as good as 1:2@60°C, which is due to the low HA' content.

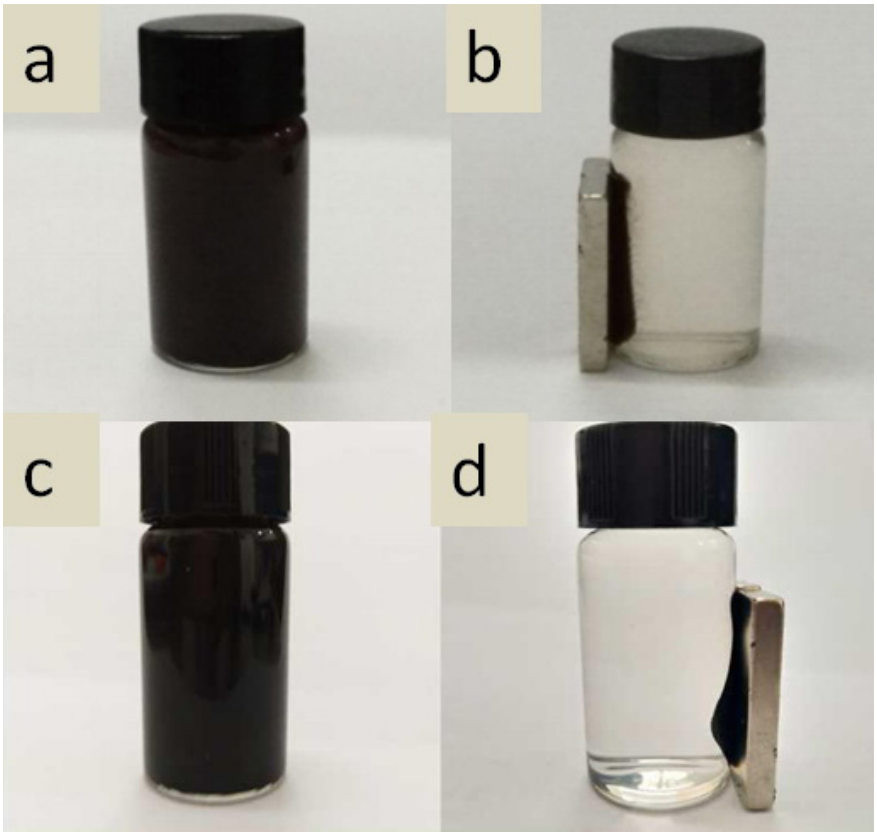

Fig. 5. Photographs of magnetic property test for M-1:1 (a,b) and 1:1@60°C (c,d).

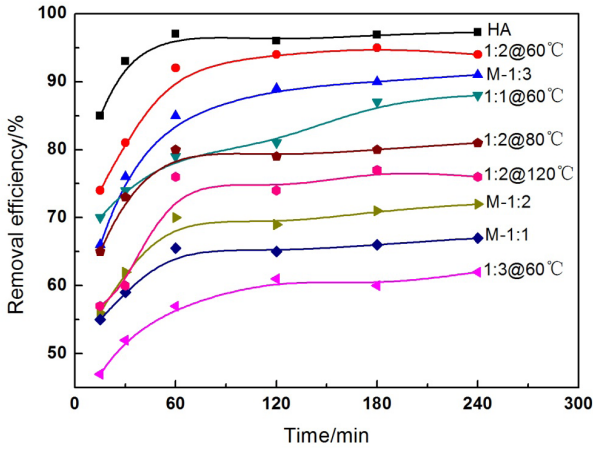

Fig. 6. The removal efficiency of bare HA and Fe_3O_4/HA synthesized mechanically and in-situ to Cu^{2+}.

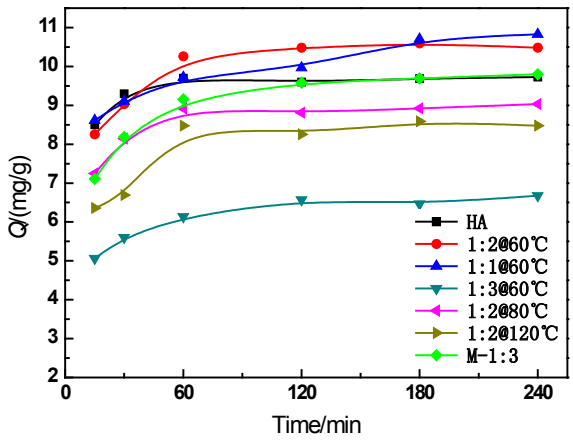

Fig. 7. The adsorption capacity of bare HA and Fe_3O_4/HA nanocomposites to Cu^{2+}.

It also can be seen that the removal efficiency of magnetic Fe_3O_4/HA nanocomposites are lower than that of bare HA. It is due to the HA' content in composites is lower than that of bare HA. Here, the adsorption capacity were calculated based on the HA content, the results are shown in Fig. 7. It can be seen that the adsorption capacity increases gradually with adsorption duration time, eventually reaching the adsorption equilibrium. Q_e of bare HA is 9.73 mg/g, that of 1:1@60°C is 10.83 mg/g, that of 1:2@60°C is 10.48 mg/g, and that of M-1:3 is 9.80 mg/g. Q_e from large to small is: 1:1@60°C > 1:2@60°C > M-1:3 > HA > 1:2@80°C > 1:2@120°C > 1:3@60°C. Therefore, it can be concluded that magnetic Fe_3O_4/HA nanocomposites synthesized in-situ has better adsorption performance than that synthesized mechanically and bare HA.

Fitting of $\ln(Q_e - Q_t)$ versus t of bare HA and Fe_3O_4/HA nanocomposites were performed according to the pseudo-first-order kinetic model (Figs. 8a,b). The pseudo-first-order adsorption rate constant k_1 of bare HA is 0.0036. The correlation coefficient R^2 is 0.31866. The experimental value of Q_e is 9.73. Its theoretical value is 4.96. The k_1 of Fe_3O_4/HA nanocomposites is 0.0221, and R^2 is 0.37475, its experimental value of Q_e is 10.60 and the theoretical value is 3.38. The first-order kinetics expresses the relationship between the occupancy rate of the adsorption sites and the number of unoccupied adsorption sites. It shows that the pseudo-first-order kinetics does not fit the adsorption of bare HA or Fe_3O_4/HA to Cu^{2+} well.

Figs. 9a and b is a pseudo-second-order kinetic fitting of bare HA andFe_3O_4/HA nanocomposites. The pseudo-second-order adsorption rate constant k_2 of bare HA is 0.061 and R^2 is 0.99993. The $k_2$of Fe_3O_4/HA is 0.023 and R^2 is 0.99964. Both correlation coefficients R^2 are more than 0.999, and the theoretical value of Q_e (HA: 9.78; Fe_3O_4/HA: 10.75) is consistent with the experimental values (HA: 9.73; Fe_3O_4/HA: 10.60), which indicates that the pseudo-second-order kinetics can describe the adsorption of bare HA and Fe_3O_4/HA nanocomposites to Cu^{2+} ions well. The adsorbent and adsorbate have electrons shared or exchanged during the adsorption rate control stage,so it is concluded that there exists ion exchange between Ca^{2+} in HA and Cu^{2+} and chemical adsorption between O^{2-} in Fe_3O_4 with Cu^{2+}.

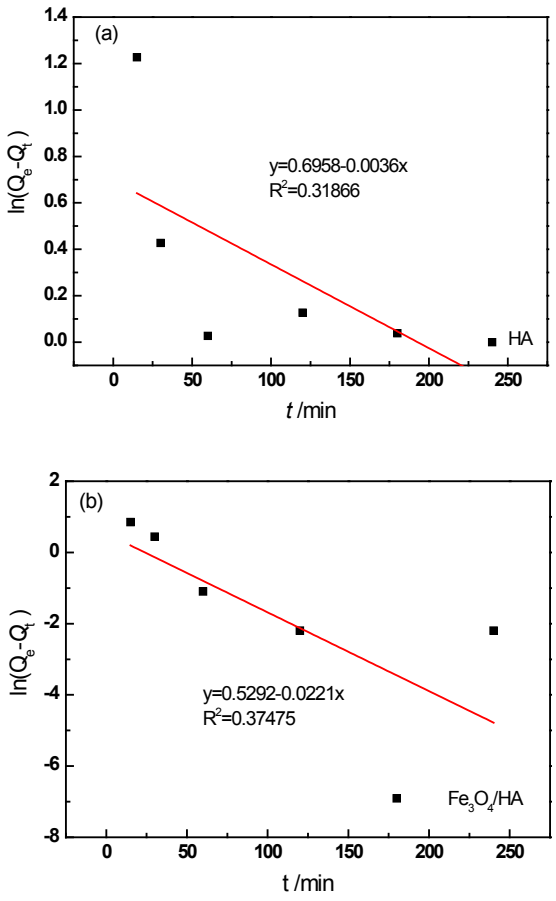

Fig. 8. The pseudo-first-order kinetic fitting of bare HA and Fe_3O_4/HA nanocomposites.

The relationship of Q_t versus $t^{1/2}$ for bare HA and Fe_3O_4/HA nanocomposites is shown in Fig. 10 (a) and (b) according to the intraparticle diffusion model, respectively. As can be seen that there are two different adsorption stages, the first stage is mainly film diffusion, and the second one is

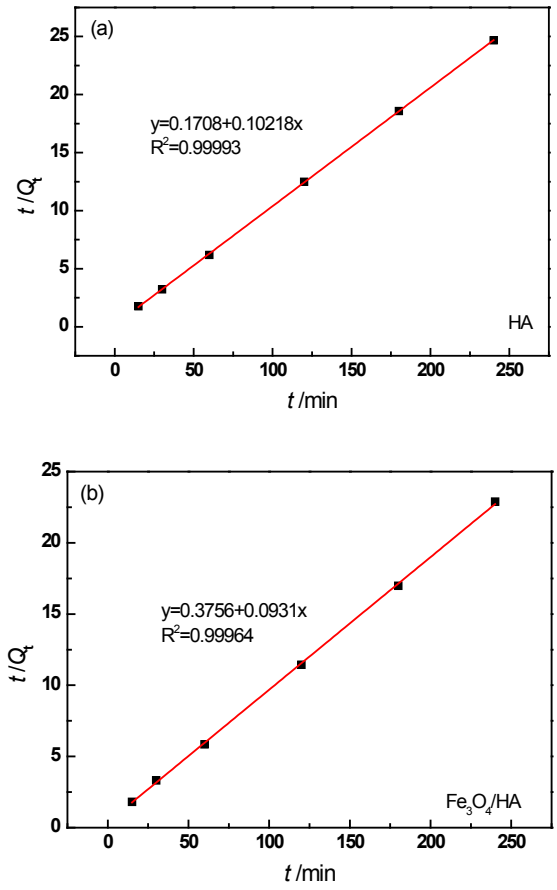

Fig. 9. The pseudo-second-order kinetic fitting of bare HA and Fe_3O_4/HA nanocomposites.

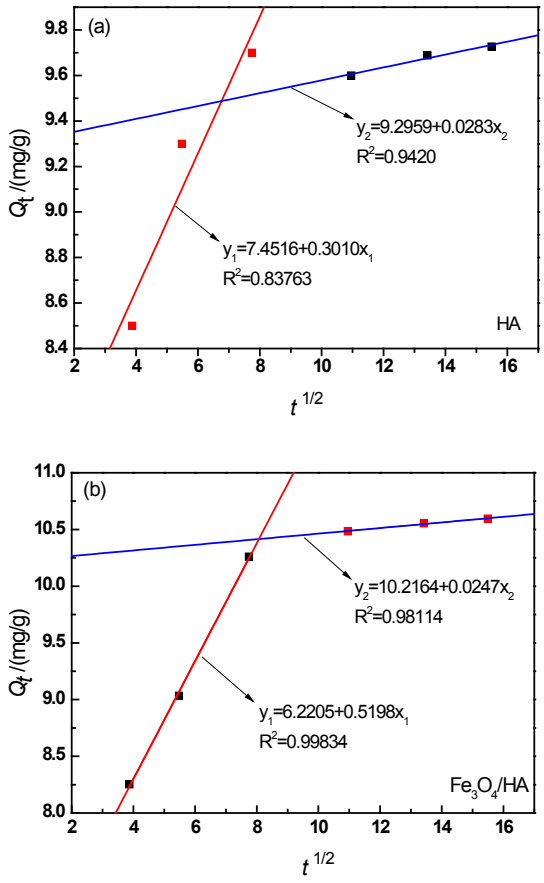

Fig. 10. The intraparticle diffusion model fitting of bare HA and Fe_3O_4/HA nanocomposites.

the internal diffusion. The k_{id1} and k_{id2} of bare HA are 0.3010 and 0.0283, respectively, and the intercepts I_1 and I_2 are 7.4516 and 9.2959, respectively; the k_{id1} and k_{id2} of Fe_3O_4/HA are 0.5198 and 0.0247, respectively and the intercepts I_1 and I_2 are 6.2205 and 10.2164, respectively. The adsorption to heavy metal ions from solution by solids is a multi-step complex process. Heavy metal ions are first adsorbed from the solution to the surface of the solid particles boundary layer and then transferred to the surface of particles through the boundary layer. So, adsorption experiences film diffusion and internal diffusion. The internal diffusion process is slow, and is usually the rate determining stage. If there is internal diffusion, then the relationship between Q_t and $t^{1/2}$ must be linear. If the internal diffusion is the rate-determining step, then the straight line need to pass the origin [26]. It can be seen from Fig. 10 that the straight line does not pass through the origin, which indicates that the adsorption process of Cu^{2+} ions by bare HA and Fe_3O_4/HA is not determined solely by internal diffusion. And the boundary layer thickness I_2 of the internal diffusion of Fe_3O_4/HA and bare HA are both larger than their boundary layer thickness I_1 of the film diffusion, and the internal diffusion rate k_{id2} are both smaller than the film diffusion rate k_{id1}, which indicates that the internal diffusion is dominant.

According to the kinetics and intraparticle diffusion model analysis, the adsorption of Fe_3O_4/HA to Cu^{2+} ions can be divided into two stages. The first stage is rapid surface adsorption, and the second is a slowly reaching adsorption equilibrium stage. The introduction of magnetic Fe_3O_4 does not change the adsorption mechanism of HA.

4. Conclusions

The Fe_3O_4/HA magnetic nanocomposites were successfully prepared by a mechanical method and an in-situ method. The magnetic Fe_3O_4/HA nanocomposites prepared mechanically are compounded with nanorod HA and spherical magnetic Fe_3O_4 in the physical way. The magnetic Fe_3O_4/HA nanocomposites synthesized in-situ are short rod-like nanoparticles, and the crystallinity degree and particle size increase with the increasement of hydrothermal temperature and molar ratio of Fe_3O_4 to HA. When the hydrothermal temperature is 60°C and the molar ratio is 1:1 (Fe_3O_4:HA), the magnetic Fe_3O_4/HA nanocomposites synthesized in-situ appear as uniform nanoparticles and good dispersibility. The morphology is more favorable to the adsorption for heavy metal ions. The magnetic Fe_3O_4/HA nanocomposites prepared by the two methods are both able to remove Cu^{2+} ions. When the ratio is 1:3 (Fe_3O_4:HA) for mechanical mixing method, the saturation removal efficiency reaches 91%. The saturation removal efficiency of

1:2@60°C in-situ reaches 95%. The equilibrium adsorption capacity of 1:1@60°C is 10.83 mg/g, higher than M-1:3 (9.80 mg/g) and bare HA (9.73 mg/g). Under the same conditions, magnetic Fe_3O_4/HA nanocomposites synthesized in-situ has better adsorption performance than that synthesized mechanically and bare HA, and easy to be separated by the external magnet field. The pseudo-second-order kinetics and intraparticle diffusion models can describe the adsorption of bare HA and magnetic Fe_3O_4/HA nanocomposites to Cu^{2+} ions well.

Acknowledgements

This work was financially supported by the Program of Natural Science Foundation of China (No. 51472166, 51272162) and Liaoning BaiQianWan Talents program.

References

[1] L. Meng, X.Y. Zhang, L.X. Pan, Discussion on treatment technologies for heavy metal wastewater, Contemp. Chem. Ind., 43 (2014) 1642–1645.
[2] R.G. Fan, Q.P. Gao, H.J. Gao, Present research situation and development of the removal of arsenic from wastewater by adsorption, Ind. Water Treat., 33 (2013) 10–12.
[3] C.F. Chang, C.Y. Chang, K.H. Chen, W.T. Tsai, J.L. Shie, Y.H. Chen, Adsorption of naphthalene on zeolite from aqueous solution, J. Colloid Interf. Sci., 277 (2004) 29–34.
[4] M. Khraisheh, Y.S. Al-Degs, W. McMinn, Remediation of wastewater containing heavy metals using raw and modified diatomite, Chem. Eng. J., 99 (2004) 177–184.
[5] Y. Sag, T. Kutsal, Determination of biosorption heats of heavy metal ions on zoogloearamigera and rhizopusarrhizus, Process Biochem., 6 (2000) 145–151.
[6] M. Ozawa, K. Satake, R. Suzuki, Removal of aqueous chromium by fishbone waste originated hydroxyapatite, Mater., 22 (2003) 513–514.
[7] C. Cooper, J.Q. Jiang, S. Ouki, Preliminary evaluation of polymeric Fe and Al-modied clays as adsorbents for heavy metal removal in water treatment, Chem. Technol. Biotechnol., 77 (2002) 546–551.
[8] M. Ayati, H.E.L. Madsen, Crystallization of some heavy-metal phosphates alone and in the presence of calcium ion, J. Crystal Growth, 208 (2000) 579–591.
[9] M.E. Hodson, E. Valsami-Jones, J.D. Cotter-Howells, Bonemeal additions as a remediation treatment for metal contaminated soil, Environ. Sci. Technol., 34 (2000) 3501–3507.
[10] A. Krestou, A. Xenidis, D. Panias, Mechanism of aqueous uranium(VI) uptake by hydroxyapatite, Miner. Eng., 17 (2004) 373–381.
[11] Z.Z. Zhang, M.Y. Li, W. Chen, L.Y. Zhu, Immobilization of lead and cadmium from aqueous solution and contaminated sediment using nano-hydroxyapatite, Environ. Pollut., 158 (2009) 514–519.
[12] T. Sriharsha, B. Dhirendra, V. Satish, N. Perkas, Z.Y. Zhong, A. Gedanken, Sonochemical stabilization of ultrafine colloidal biocompatible magnetite nanoparticles using amino acid, L-arginine, for possible bioapplications, Ultrason. Sonochem., 17 (2010) 730–737.
[13] T. Ugur, G. Yusuf, H.B. Ismail, Synthesis of magnetic core-shell Fe_3O_4-Au nanoparticle for biomolecule immobilization and detection, J. Nanopar. Res., 12 (2010) 1187–1196.
[14] C.L. Wu, H. He, H.J. Gao, G. Liu, R.J. M, Y.L. An, L.Q. Shi, Synthesis of Fe_3O_4@SiO_2@polymer nanoparticles for controlled drug release, Sci. China Chem., 53 (2010) 514–518.
[15] L.A. Cano, E.D. Cabanillas, S.G. Marchetti, Synthesis and characterization of superparamagnetic iron oxide nanoparticles forbiomedical applications, Hyperfine Interact., 195 (2010) 275–280.
[16] S. Panseri, C. Cunha, T. D'Alessandro, M. Sandri, A. Russo, G. Giavaresi, M. Marcacci, C.T. Hung, A. Tampieri, Magnetic hydroxyapatite bone substitutes to enhance tissue regeneration: evaluation in vitro using osteoblast-like cells and in vivo in a bone defect, Plos One, 6 (2012) 1–8.
[17] Z. Chen, Y.H. Li, Preparation of magnetic ferriferous oxide and its application in purification of heavy metal ions in waste water, Inorg. Chem. Ind., 47 (2015) 20–22.
[18] K. Mahmud, M.A. Islam, A. Mitsionis, T. Albanis, T. Vaimakis, Adsorption of direct yellow 27 from water by poorly crystalline hydroxyapatite prepared via precipitation method, Desal. Water Treat., 41 (2012) 170–178.
[19] N. Barka, S. Qourzal, A. Assabbane, A. Nounah, Y. Ait-Ichou, Removal of reactive yellow 84 from aqueous solutions by adsorption onto hydroxyapatite, J. Saudi Chem. Soc., 15 (2011) 263–267.
[20] S.H. Wang, H. Wang, Z.X. Hou, X.D. Hu, C.L. Niu, Z.L. Xue, H. Wang, C. Wang, Crystal growth and crystallinity of nano-hydroxyapatite prepared by sol-gel, Rare Metal Mater. Eng., 40 (2011) 44–47.
[21] S.H. Wang, C. Wang, Z.X. Hou, H. Wang, X.D. Hu, H.R. Lu, Z.L. Xue, C.L. Niu, Reverse microemulsion synthesis of hydroxyapatite nanoparticles and adsorption performance study, Key Eng. Mater., 512–515 (2012) 119–122.
[22] S.H. Wang, H. Wang, Z.X. Hou, C. Wang, X.D. Hu, H.R. Lu, Z.L. Xue, C.L. Niu, Preparation and properties of nano-hydroxyapatite derived from sol-gel method for Cu^{2+} polluted water, Key Eng. Mater., 512–515 (2012) 115–118.
[23] S.H. Wang, J.G. Xia, M.H. Wang, Z.X. Hou, D. Zhou, L.D. Zhou, Preparation and adsorption property of nano-rods hydroxyapatite using cationic surfactant templates, Adv. Mater. Res., 771 (2013) 109–112.
[24] Y.T. Guan, S.H. Wang, M.H. Wang, Z.X. Hou, X.D. Hu, H. Wang, H.L. Fan, N. Zhang, Effect of initial concentration of Cu^{2+} on the adsorption performance of hydroxyapatite, Adv. Mater. Res., 989–994 (2014) 312–315.
[25] C. Wang, Z.X. Hou, M.H. Wang, H. Wang, J.G. Xia, Y.T. Guan, S.H. Wang, The research on preparation and adsorption Cu^{2+} property of PAM modification HA, Funct. Mater., 45 (2014) 02059–02062.
[26] G. Mckay, Y.S. Ho, Peseudo-second-order model for sorption processes, Process. Biochem., 34 (1999) 451–456.